A STUDY OF METHODS USED IN

# MEASUREMENT AND ANALYSIS OF SEDIMENT LOADS IN STREAMS

REPORT II

PROGRESS REPORT

ON

TEMPERATURE EFFECTS IN VIBRATIONAL-TYPE

SEDIMENT-CONCENTRATION GAGES

1987

REPORT II PROGRESS REPORT ON TEMPERATURE EFFECTS IN VIBRATIONAL-TYPE SEDIMENT-CONCENTRATION GAGES

A Study of Methods Used in

MEASUREMENT AND ANALYSIS OF SEDIMENT LOADS IN STREAMS

A Cooperative Project

Sponsored by the

Interagency Advisory Committee on Water Data

Subcommittee on Sedimentation

Participating Agencies

Agricultural Research Service
Corps of Engineers ** Geological Survey
Forest Service ** Bureau of Reclamation
Federal Highway Administration ** Bureau of Land Management

REPORT II

# PROGRESS REPORT

# ON

# TEMPERATURE EFFECTS IN VIBRATIONAL-TYPE SEDIMENT-CONCENTRATION GAGES

By John V. Skinner

Prepared for Publication by the Staff of the
Federal Inter-Agency Sedimentation Project
St. Anthony Falls Hydraulic Laboratory
Minneapolis, Minnesota

Published by
U.S. Army Engineer District, St. Paul

1987

CONTENTS


| | Page |
|---|---|
| Abstract | 1 |
| Introduction | 2 |
| Purpose and scope | 4 |
| Terminology | 4 |
| Theory of vibrating tubes | 7 |
| Equations of motion | 7 |
| Auxiliary-equation roots | 12 |
| Boundary conditions | 14 |
| Tension-equation roots | 18 |
| Special solutions of the tension equation | 23 |
| Analysis of experimental data | 30 |
| Parameters for the straight-tube sediment gage | 33 |
| Comparison of measured frequencies and theoretical frequencies | 39 |
| Temporal shifts in frequency | 43 |
| Conclusions | 44 |
| Appendix A - notation | 46 |
| References | 48 |

## ILLUSTRATIONS


| | | | Page |
|---|---|---|---|
| Figure | 1. | Modal shapes for a tube clamped at both ends | 6 |
| | 2. | Forces influencing vibrational frequencies | 8 |
| | 3. | Location of auxiliary-equation roots | 13 |
| | 4. | Coordinate system for a vibrating tube | 13 |
| | 5. | Secant method for locating tension-equation roots | 19 |
| | 6. | Program listing for the secant method | 21 |
| | 7. | Sample outputs from the secant-method program | 22 |
| | 8. | Roots of the tension equation | 24 |
| | 9. | Tension-compression regions for three modes of vibration | 26 |
| | 10. | Straight-tube sediment gage | 31 |
| | 11. | Tube vibrating in its first mode and carrying a concentrated mass | 34 |
| | 12. | Comparison of measured and theoretical frequencies | 40 |
| | 13. | Detail of tension-compression curve for first mode | 45 |


## TABLES


| | | | |
|---|---|---|---|
| Table | 1. | Comparison of vibrational frequencies for the special case, S = 0 | 27 |
| | 2. | Vibrational constants for various temperatures | 38 |

## ABBREVIATIONS AND CONVERSION FACTORS

For the use of readers who prefer to use inch-pound units, conversion factors for metric terms used in this report are listed below:

| Multiply metric unit | by | To obtain inch-pound unit |
|---|---|---|
| | Length | |
| millimeter (mm) | 0.03937 | inch (in.) |
| meter (m) | 3.281 | foot (ft) |
| | Volume | |
| liter (L) | 0.2642 | gallon (gal) |
| | Speed | |
| meter per second (m/s) | 3.281 | foot per second (ft/s) |
| | Mass | |
| gram (g) | 0.002205 | pound (lb) |
| kilogram (kg) | 2.205 | pound (lb) |
| | Force | |
| Newton (N) | 0.2248 | pound (lb) |

Temperature

Temperature in degrees Fahrenheit ($^{o}$ F) can be converted to degrees Celsius ($^{o}$ C) as follows:

$$^{o}\,F = 1.8^{o}\,C + 32$$

| | | |
|---|---|---|
| | Density | |
| gram per cubic centimeter ($g/cm^3$) | 0.03613 | pound per cubic inch ($lb/in^3$) |
| | Pressure | |
| kilopascal (kPa) | 0.1450 | pound per square inch ($lb/in^2$) |

# PROGRESS REPORT

# ON

# TEMPERATURE EFFECTS IN VIBRATIONAL-TYPE SEDIMENT-CONCENTRATION GAGES

By

John V. Skinner

## ABSTRACT

An experimental gage for measuring sediment concentrations in flowing water was designed and then tested under laboratory conditions. The gage consists of a steel tube girdled at both ends by ring-shaped weldments that join with a waterproof housing. The outside of the tube is shielded by the housing but the inside of the tube can be filled with slurries of flowing, sediment-laden water. Electromagnets inside the housing cause the tube, water, and sediment to oscillate like a vibrating violin string.

The measurement principle is based on the relation between vibrational frequency and concentration of sediment in the slurry. As concentration increases, the slurry becomes denser and the tube vibrates at a lower frequency. A measurement is made by reading the frequency and then using a calibration chart to convert frequency to concentration.

Tests show the experimental gage has two undesirable characteristics: frequency is strongly influenced by water temperature, and frequency slowly shifts over time. Correcting these problems will require redesign based on quantitative assessments of factors controlling the gage's response. To aid design work, the paper presents equations that relate frequency to (a) water

density, (b) sediment density, (c) sediment concentration, and (d) properties of the tube itself. These properties include thermal-expansion coefficient, elasticity, tube diameter, tube length, and tension forces in the metal walls. Theoretical results indicate the tensive forces are offending factors that produce temperature instabilities and drift problems. The forces probably evolved during the process of arc welding the tube and housing together.

## INTRODUCTION

Fluvial sediment can adversely affect waterways, lakes, and estuaries. Soil particles dislodged by rain, flowing water, and landslides may damage fish-spawning areas, fill navigation channels, and reduce storage space in reservoirs. On the other hand, sediment is beneficial in certain instances. Ocean beaches are created and replenished by sediment from nearby estuaries. If sediment supplies are disrupted, wave action erodes the beaches and exposes underlying strata of soil or rock.

Sediment studies require field data which are difficult and expensive to collect. Technicians must travel to sampling sites, collect water specimens, then ship the specimens to laboratories where sediment concentrations can be determined. Several months may pass before the laboratory data are available for engineering analysis.

One way of simplifying and speeding the data-collection processes is to install electronic sediment-concentration gages at monitoring sites and link the gages to a central office by means of radio or telephone. An experimental gage of this type was tested at a field site near Madison,

Wisconsin (Skinner et al., 1986). The instrument consisted of a tube that oscillated at frequencies determined by the concentration of sediment in the river water. Preliminary tests showed the gage met requirements for speed and accuracy; however, the shape of the vibrating tube created certain problems. Because the tube was bent into a "U" shape with both ends facing the same direction, the gage was unsuitable for underwater applications. Water would not flow through the tube if it was submerged. To overcome this problem, the gage was mounted above water and connected to a submerged sampling pump. At Madison, pumping solved the problem of supplying water to the vibrating U-tube gage; however at many other sites, pumping is impossible because electricity is not available.

Pumps create another problem related to the fixed intakes. Concentrations of suspended sediment vary from point to point in a river's cross section. For example, concentrations near the bed of a river generally exceed concentrations near the water surface. Data on concentration gradients are important; however, this information is not registered by a U-tube which must sample from a fixed point. The sampling pump, along with its intake, electric cord, and tubing are too cumbersome to move around in the cross section.

Another sampling problem stems from opposing requirements for pumping rates. To minimize frequency-measurement errors, pumping rates must be stable; however, to minimize sediment sampling errors, pumping rates must be constantly adjusted to match flow-velocities at the intake.

Striving to overcome disadvantages of the U-shaped tube, personnel at the Sedimentation Project built an experimental sediment gage that contains

a straight vibrating tube. This new instrument can be submerged and moved in a cross section to map concentration gradients. Because the tube is open at both ends, flow rates approaching the tube are only slightly greater than flow rates inside the tube. However, laboratory tests revealed two problems. Frequencies slowly shift with the passage of time and frequencies are strongly influenced by water temperature.

## Purpose and Scope

The purpose of this study is to derive equations for designing an improved version of the straight-tube sediment gage. The scope of this study is limited to analyzing natural frequencies of a tube with its ends rigidly clamped to immovable supports.

## Terminology

External forces play an important role in setting a tube's vibrational frequencies. Consider a slender tube mounted horizontally with its ends clamped to stationary supports. Any external force that alternately pushes down and pulls up on the tube causes it to vibrate. Furthermore, the frequency of vibration matches the frequency of the external force. This type of motion is termed *forced vibration*.

If external forces are absent, a tube can still be made to vibrate. To initiate vibration, the tube must be pushed away from its rest position and then released suddenly. Striking the tube a sharp blow provides the required stimulus and starts a form of motion termed *free vibration*. Motion occurs only at certain *natural* frequencies set by the tube's shape, size,

mass, length, and rigidity. A perfectly-elastic tube vibrating in a vacuum can bend and relax without losing energy so the motion continues forever.

The term *damping* refers to the process of removing energy from a vibrating tube. In most tubes, kinetic energy is transformed to heat through the action of friction forces. Some friction occurs within the tube's walls: the remainder occurs outside the tube as air shifts back and forth around the moving tube surface.

A vibrating tube alternately bends and straightens as it shifts through each vibrational cycle. A cycle begins with the tube arched into one of its *modal* shapes. From this starting point, the tube makes a series of moves. After straightening, the tube bends into a mirror image of its modal shape. The tube then straightens again and finally completes the cycle by returning to its original shape.

A tube can vibrate in many modes. Figure 1a shows the first mode as three sets of lines representing snapshots of the tube as it shifts through a cycle. As the tube oscillates, all points along its axis move down together and then move up together. In common parlance, we say the points move *in phase* with one another.

The second modal shape is shown in figure 1b. The tube vibrates in two segments: one segment is left of the midpoint and the other segment is to the right. The opposing arrows show the phase relation between two segments. During the first half cycle, the left segment shifts down while the right segment shifts up. During the last half cycle, the left segment shifts up while the right segment shifts down. In common parlance, we say the segments move in *phase opposition* with one another.

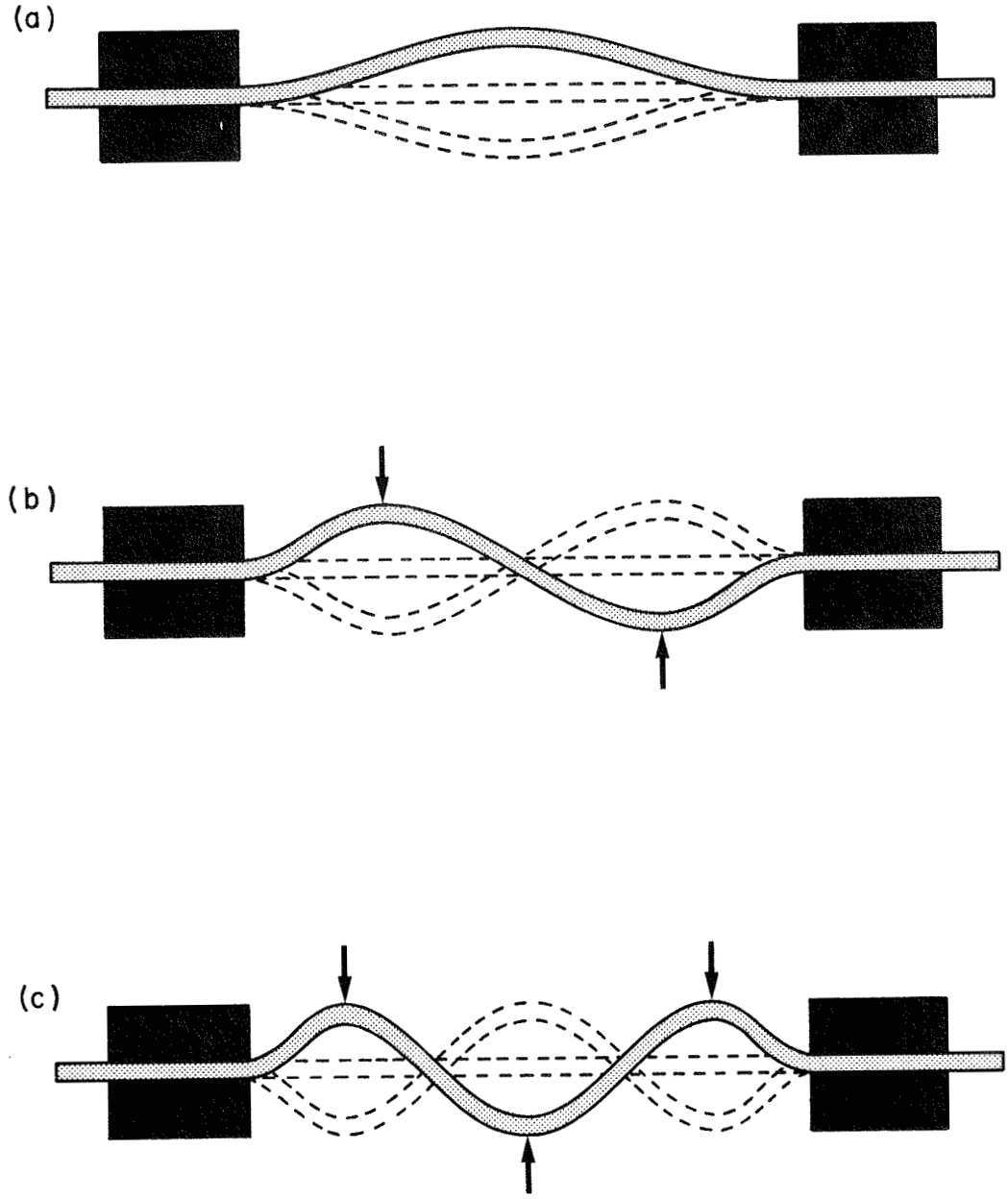


Figure 1.--Modal shapes for a tube clamped at both ends. (a) First modal shape. (b) Second modal shape. (c) Third modal shape.

The third modal shape is shown in figure 1c. The tube vibrates in three segments. Adjacent segments move in phase opposition with one another.

In theory a tube has an infinite number of modal shapes; however, in discussions that follow, we will focus on the first, second, and third modes.

## THEORY OF VIBRATING TUBES

In this section, we formulate equations describing the movement of vibrating, liquid-filled tubes. The first two topics--*equations of motion* and *auxiliary-equation roots*--cover general cases: no restrictions are imposed on the tube's end supports. The next three topics--*boundary conditions*, *tension-equation roots*, and *special solutions of the tension equation*--are more restrictive: only tubes having rigid end supports are considered.

### Equations of Motion

Figure 2a shows a tube mounted between two fixed supports that encircle the tube like snug-fitting collars. These supports (a) prevent the tube's ends from moving vertically but (b) allow the ends to slide horizontally. The S forces, which pull on the ends of the tube, act on the entire length of tube including the section between the fixed supports. For simplicity, the tube is shown in its first mode; however, the discussion in this section applies to all modes.

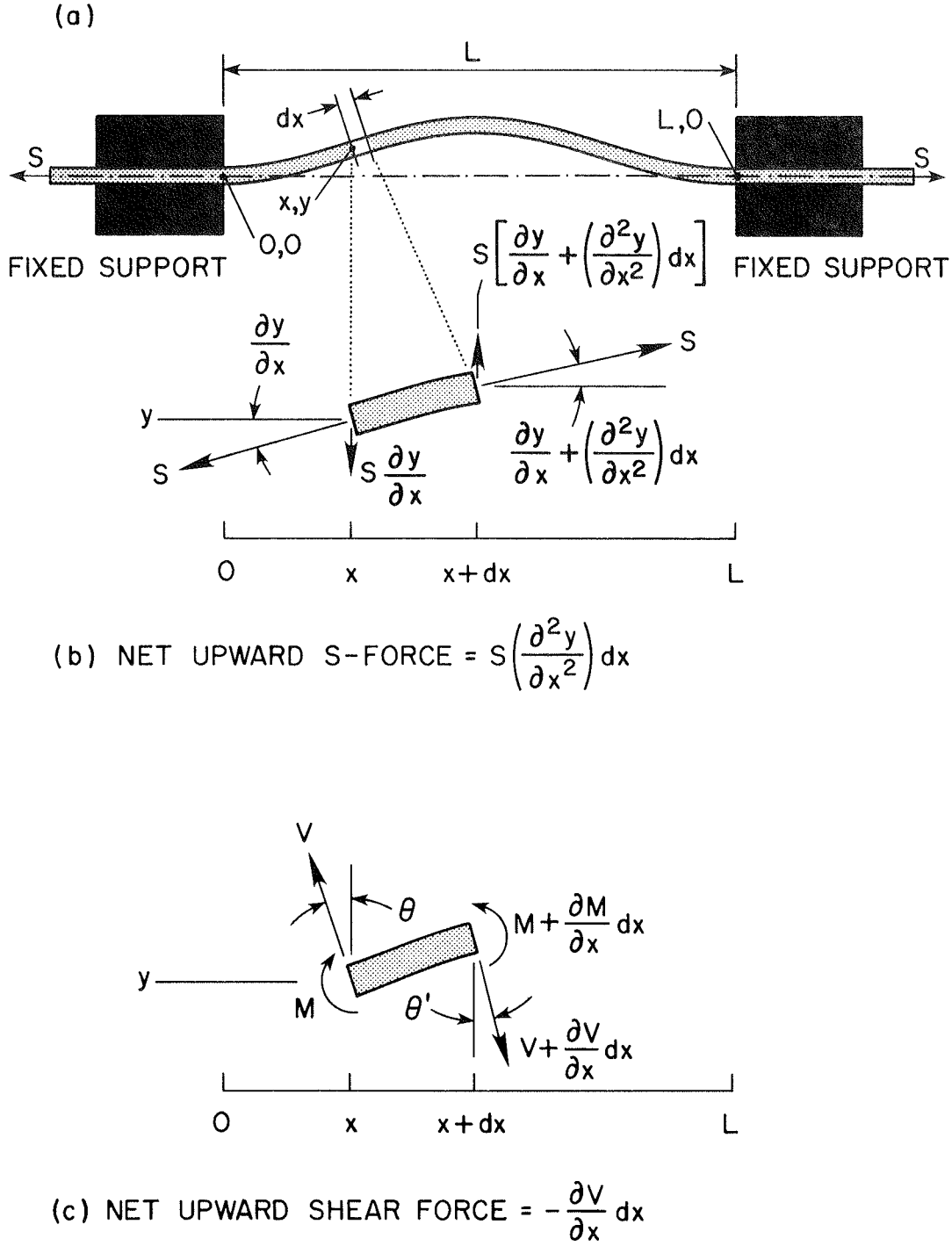


Figure 2.--Forces influencing vibrational frequencies. (a) Axial forces on tube ends. (b) Axial forces on a tube element. (c) Bending and shear forces on a tube element.

Equations for the tube's motion will be based on the following assumptions:

(a) Any chosen point on the tube (figure 2a) moves up and down with pure harmonic motion. In other words, the motion is of the form $y = \sin(pt)$ where p is angular frequency, t is elapsed time, and y is the point's displacement measured from a stationary reference line passing through the support centers.

(b) Every cross section normal to the tube's axis is acted upon by the force S.

(c) The maximum vertical displacement of any point on the tube's axis is much smaller than the length "L."

(d) All cross sections are identical: the tube is uniform from end to end.

(e) The tube is free of all damping forces.

(f) Rotational movement of tube sections can be neglected.

We now apply Newton's second law of motion to a tube section between x and x+dx. Our objective is to equate the net upward force acting on this section to the mass of the section multiplied by its upward acceleration.

We divide the equation-writing process into two phases. In the first phase, we focus on the axial force S. Figure 2b (a) shows all vertical forces acting on the section ends and (b) gives the net upward force which is the sum of all upward forces minus the sum of all downward forces. In the second phase, we focus on shear forces, "V," acting on the section ends. Figure 2c shows the shear-force vectors are normal to the tube's axis and therefore slightly inclined to the y axis. Because the inclination angles $\theta$ and $\theta'$ are small (see assumption "c"), the functions $\cos(\theta)$ and $\cos(\theta')$

are nearly equal to 1. Therefore, the vertical components of the shear forces are obtained by simply rotating the original shear vectors into the y axis. Subtracting the right-hand shear force, which acts downward, from the left-hand force, which acts upward, we obtain the net upward-shear force expression on figure 2c.

The tube section has a mass of r(dx) and an upward acceleration of $\partial^2 y/\partial t^2$ (refer to Appendix A for definition of symbols). Mass, acceleration, and net upward force (see figure 2b and 2c) are related as follows:

$$r(dx)(\partial^2 y/\partial t^2) = S(dx)(\partial^2 y/\partial x^2) - (dx)(\partial V/\partial x) \qquad (1)$$

Equation 1 can be written in a more convenient form by applying an assumption and then relating bending moments to shear forces. Each of the two S-forces (figure 2b) produces a moment: one moment acts clockwise and the other acts counterclockwise. In general, these two moments do not cancel because the moment arms are not equal. An exact analysis must include the net moment; however, this discussion neglects the net moment as stated in assumption "f."

The two shear forces (straight arrows on figure 2c) share a common moment arm of dx/2 measured from the element's center point. Furthermore, each force produces a clockwise moment. The two bending moments (curved arrows on figure 2c) differ in magnitude but oppose one another in direction. With these facts in mind, we equate clockwise moments to counterclockwise moments. As an approximation, we drop terms involving high-order differentials to obtain $V = \partial M/\partial x$. This equation is differentiated with respect to x to obtain $\partial V/\partial x = \partial^2 M/\partial x^2$--we now have the

first of two equations required to simplify equation 1. The other equation, $\partial^2 M/\partial x^2 = EI(\partial^4 y/\partial x^4)$, is obtained by taking the second derivative of the bending-moment equation, $M = EI\partial^2 y/\partial x^2$, derived by Laurson and Cox (1947).

The equations $\partial V/\partial x = \partial^2 M/\partial x^2$ and $\partial^2 M/\partial x^2 = EI\partial^4 y/\partial x^4$ contain the common term $\partial^2 M/\partial x^2$. Eliminating this term by combining the two preceding equations yields $\partial V/\partial x = EI\partial^4 y/\partial x^4$. The expression for $\partial V/\partial x$ is now substituted into equation 1 and then the factor dx is canceled. We obtain:

$$r(\partial^2 y/\partial t^2) - S(\partial^2 y/\partial x^2) + EI(\partial^4 y/\partial x^4) = 0. \qquad (2)$$

The next part of the analysis involves the modal-shape function "X," which defines the shape of the tube's axis when the tube reaches its maximum deflection. X is a function of only one variable--namely x. An expression for y, the deflection of any chosen point on the tube's axis, must obviously involve both x and t (time). According to assumption "a," the vibratory up-and-down motion is harmonic and is represented by the expression sin(pt). Multiplying this expression by X gives the general deflection equation, $y = X \sin(pt)$. Partial derivatives of y can now be written as follows:

$\partial^2 y/\partial t^2 = -Xp^2 \sin pt$; $\partial^2 y/\partial x^2 = (\partial^2 X/\partial x^2) \sin pt$; $\partial^4 y/\partial x^4 = (\partial^4 X/\partial x^4) \sin pt$.

By substituting these partial derivatives into equation 2, and then cancelling the sin (pt) factors, we obtain

$$EI\ (\partial^4 X/\partial x^4) - S\ (\partial^2 X/\partial x^2) - Xrp^2 = 0 \qquad (3)$$

The partial derivatives in equation 3 can be replaced with total derivatives because X is a function of x alone. After completing this substitution, we obtain the linear differential equation:

$$EI\ (d^4 X/dx^4) - S\ (d^2 X/dx^2) - Xrp^2 = 0. \qquad (4)$$

## Auxiliary-equation Roots

We now use the "auxiliary-equation method" described by Leighton (1952, p. 47) to solve equation 4. First substitute the "D-operator," defined as $D = d/dx$, into equation 4 and then factor the parameter X. We obtain

$$X(EID^4 - SD^2 - rp^2) = 0 \tag{5}$$

The auxiliary equation is formed by setting the expression in parentheses equal to zero. After dividing all terms by EI, we obtain

$$D^4 - (S/EI)D^2 - rp^2/EI = 0 \tag{6}$$

Equation 6, being a fourth-order polynomial, has four roots. Assuming two of the roots are real--call them a and a'--and two are conjugate imaginary--call them +jb and -jb, we write equation 6 in factored form as follows:

$$(D-a)(D-a')(D+jb)(D-jb) = 0 \tag{7}$$

After multiplying these factors together and collecting common terms, we obtain

$$D^4-(a+a')D^3 + (b^2+aa')D^2 - (a+a')b^2D + aa'b^2 = 0 \tag{8}$$

The real roots of equation 6 are related to one another. Notice that terms involving $D^3$ and D are not present in equation 6 and that these terms vanish from equation 8 if $a' = -a$. Apparently, the two real roots of equation 6 are equal in magnitude but opposite in sign. The four roots of equation 6 and their positions in the complex plane are shown in figure 3.

According to Leighton (1952), the general solution of equation 4 can now be written in terms of the auxiliary-equation roots. The roots (see figure 3) become exponents and the general solution has the form

$$X = C_1e^{ax} + C_2e^{-ax} + C_3e^{+jbx} + C_4e^{-jbx} \tag{9}$$

The coefficients $C_1$, $C_2$, $C_3$, and $C_4$ are arbitrary constants.

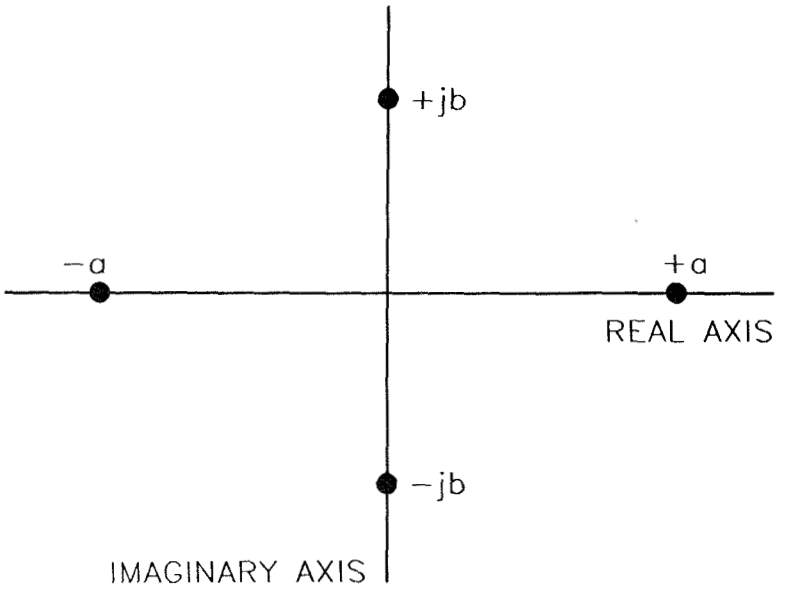


Figure 3.--Location of auxiliary-equation roots.

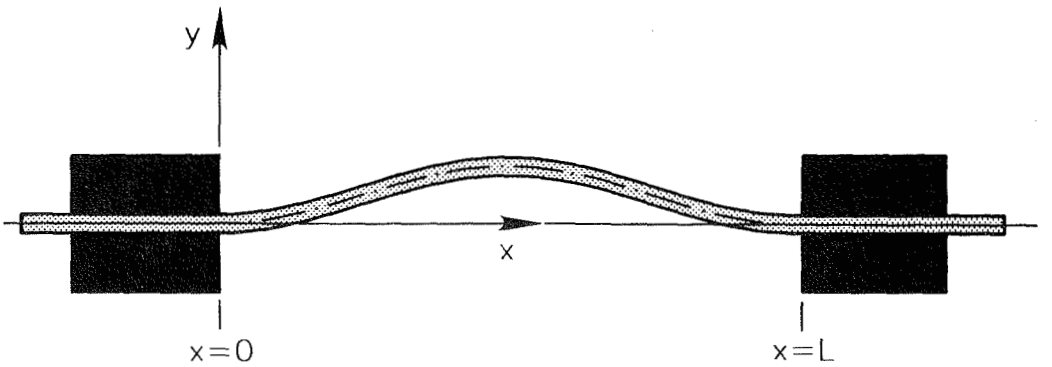


Figure 4.--Coordinate system for a vibrating tube.

## Boundary Conditions

Equation 4 and its solution (equation 9) were derived without specifying the type of supports at the tube's ends; therefore, the equations cover a broad variety of situations. Many forms and combinations of end supports (boundary conditions) are possible. For example, one end of a tube can be clamped and the other end can be free. Timoshenko et al. (1974, p. 454) solved equation 4 for a tube with both ends resting on knife-edge supports. The ends rocked clockwise and then counterclockwise as the center point translated up and down. Timoshenko's solution does not apply to the clamped-end arrangement shown on figure 1; however, his technique for obtaining solutions can be applied to the problem at hand.

First, we align the tube with the coordinate system on figure 4. Deflections of points on the tube's axis are measured from the tube's rest position denoted by the short-dashed line. The tube's left end lies at $x = 0$ and the right end lies at $x = L$. The modal-shape function X defines the relation between y and x through the range $0 \leq x \leq L$.

Two pairs of boundary-condition equations are required to obtain a solution. The first pair stems from constraints on translation. At $x = 0$, the tube cannot translate up and down; therefore, the condition $X = 0$ must be satisfied. After substituting 0 for both X and x in equation 9, we obtain

$$C_1 + C_2 + C_3 + C_4 = 0 \tag{10}$$

At $x = L$, the tube cannot translate up and down; therefore, the condition $X = 0$ must be satisfied. After substituting 0 for X and then substituting L

for x in equation 9, we obtain

$$C_1e^{aL} + C_2e^{-aL} + C_3e^{jbL} + C_4e^{-jbL} = 0 \tag{11}$$

The second pair of boundary-condition equations stem from constraints on rotation: no rocking motion can occur at the ends. Notice that the tube's axis (fig. 4) forms a smooth curve that starts as a horizontal line inside the left clamp. The axis arches across the region between the clamps and then terminates as a horizontal line inside the right clamp. Between the clamps, the axis shifts with the passage of time; however, at x = 0 and at x = L, the axis always coincides with the rest position. Stated mathematically, at x = 0 and at x = L the slope of the modal-shape function, dX/dx, must be zero.

Differentiating equation 9, we obtain

$$dX/dx = aC_1e^{ax} - aC_2e^{-ax} + jbC_3e^{jbx} - jbC_4e^{-jbx} \tag{12}$$

After substituting zero for x and dX/dx in equation 12, we obtain

$$aC_1 - aC_2 + jbC_3 - jbC_4 = 0 \tag{13}$$

Returning to equation 12, we substitute L for x and then substitute 0 for dX/dx to obtain

$$aC_1e^{aL} - aC_2e^{-aL} + jbC_3e^{jbC} - jbC_4e^{-jbL} = 0 \tag{14}$$

Equations 10, 11, 13, and 14 form a homogenous system with four unknowns--$C_1$, $C_2$, $C_3$, and $C_4$. Rothenberg (1983, p. 116) shows the system has non-zero solutions only if the determinant formed from the coefficients

of $C_1$, $C_2$, $C_3$, and $C_4$ is zero. Setting up the determinant, we obtain:

$$\begin{vmatrix} 1 & 1 & 1 & 1 \\ e^{aL} & e^{-aL} & e^{jbL} & e^{-jbL} \\ a & -a & jb & -jb \\ ae^{aL} & -ae^{-aL} & jbe^{jbL} & -jbe^{-jbL} \end{vmatrix} = 0 \qquad (15)$$

To solve equation 15, we expand the determinant into a polynomial. Rothenberg (1983, p. 100) and most algebra texts describe the process so only a few intermediate steps are given here. By multiplying rows in equation 15 by constants and replacing rows with the sum of two other rows, we manipulate the determinant into the following form which contains leading zero's in all but the first row:

$$\begin{vmatrix} 1 & 1 & 1 & 1 \\ 0 & 1-e^{-2aL} & 1-e^{-aL+jbL} & 1-e^{-aL-jbL} \\ 0 & ae^{-2aL}-a & jb-jbe^{-aL+jbL} & -jb+jbe^{-aL-jbL} \\ 0 & 1+e^{-2aL} & 1-j(b/a)e^{-aL+jbL} & 1+j(b/a)e^{-aL-jbL} \end{vmatrix} = 0 \qquad (16)$$

At this point, let us introduce parameters f and g and define them as follows:

$$f = aL \qquad (17)$$

$$g = bL \qquad (18)$$

We now substitute f and g into the determinant of equation 16 and then expand the determinant about its left column. Because this column contains three zeros, the 4 x 4 determinant reduces to the following 3 x 3 determinant:

$$\begin{vmatrix} 1-e^{-2f} & 1-e^{-f+jg} & 1-e^{-f-jg} \\ e^{-2f}-1 & +j(g/f)-j(g/f)e^{-f+jg} & -j(g/f)+j(g/f)e^{-f-jg} \\ 1+e^{-2f} & 1-j(g/f)e^{-f+jg} & 1+j(g/f)e^{-f-jg} \end{vmatrix} = 0 \qquad (19)$$

The 3x3 determinant in equation 19 can be expanded into a polynomial by applying the following identity:

$$\begin{vmatrix} A & B & C \\ D & E & F \\ G & H & I \end{vmatrix} = AEI+BFG+CHD-CEG-BDI-AHF \tag{20}$$

The polynomial expansion of equation 19 contains terms with complex (mixture of real and imaginary) exponents. Each of these complex terms can be written as the sum of two other terms--one entirely real and the other entirely imaginary. The following two identities are used repeatedly in this process:

$$e^{f+jg} = e^{f}e^{jg} \tag{21}$$

and

$$e^{jg} = \cos(g)+j\ \sin(g) \tag{22}$$

The next step consists of sorting terms in the polynomial expansion. Two groups are formed: one contains only real terms and the other contains only imaginary terms. The real-term group reduces to zero and the imaginary-term group contains the common factor +j. After multiplying the imaginary-term group by -j and recalling that (+j)(-j) = 1 and (-j)(0) = 0, we obtain the following:

$$-2(g/f)e^{-f}\cos(g) + 4(g/f)e^{-2f} - 2(g/f)e^{-3f}\cos(g) - (g/f)^2e^{-f}\ \sin(g)$$
$$+ (g/f)^2e^{-3f}\sin(g) - e^{-3f}\sin(g) + e^{-f}\sin(g) = 0 \tag{23}$$

Equation 23, can be simplified and rewritten as

$$[1-(g/f)^2][e^{f}-e^{-f}]\ \sin(g) - 2(g/f)(e^{f}+e^{-f})\cos(g) + 4(g/f) = 0 \tag{24}$$

In discussions that follow, equation 24 will be referred to as the "tension equation."

## Tension-equation Roots

In this section, we solve for f and g values that satisfy the tension equation. Let P represent the expression left of the equal sign in equation 24. After assigning a fixed (but arbitrary) value to f, we evaluate P for a range of g values and then plot P versus g. The plot (not shown) forms a smooth, sinuous curve that intersects the g axis an infinite number of times. Each intersection point satisfies the condition P = 0 and therefore locates a root.

Figure 5, which shows a small section of the P-versus-g curve (solid line), illustrates the root-finding technique. A root, shown by the open circle, is located by a process of successive approximations. The first approximation starts with two estimates of the root. One estimate, which is labeled $g_{i-1}$, is termed the "old" estimate. The other, which is labeled $g_i$, is termed the "current" estimate. An equation discussed in the following section is used to evaluate a "new" estimate, labeled $g_{i+1}$. The new estimate lies at the intersection of the "g" axis and the dashed line drawn through the old and current estimates. This new estimate usually lies closer to the true root than either the old or current estimates.

The equation for computing $g_{i+1}$ is based on the two shaded triangles on figure 5. Because the triangles are similar, the ratio of matching sides can be equated as follows:

$$[P(g_{i-1}) - P(g_i)] / P(g_i) = (g_{i-1} - g_i)/(g_i - g_{i+1}) \tag{25}$$

After cross-multiplying and solving for $g_{i+1}$, we obtain

$$g_{i+1} = g_i - P(g_i)[(g_i - g_{i-1})/(P(g_i) - P(g_{i-1})] \tag{26}$$

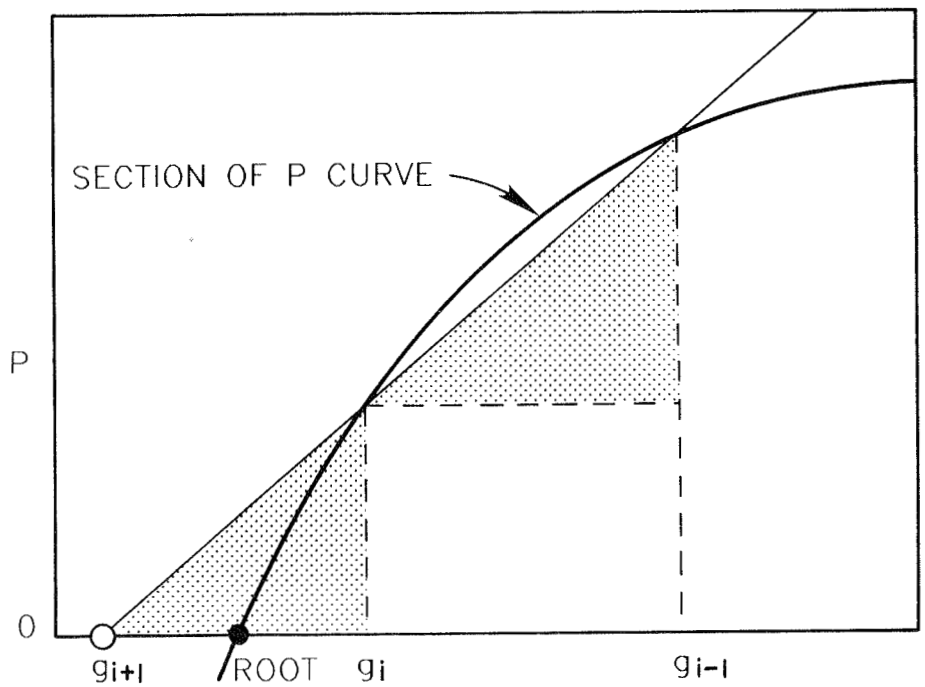


Figure 5.--Secant method for locating tension-equation roots.

Notice that the right side of equation 26 contains the old and current estimates along with two P values, $P(g_{i-1})$ and $P(g_i)$, which can be computed from the left-hand expression in equation 24.

After computing $g_{i+1}$ from equation 26, the root estimates are updated and relabeled. The value of $g_i$ is relabeled $g_{i-1}$ and the value of $g_{i+1}$ is relabeled $g_i$. The original value of $g_{i-1}$ is discarded. Stated another way; the three g-values are shifted backward in time and the oldest g value is thrown away. Another iterative process is now started by returning to equation 26 and evaluating a new value for $g_{i+1}$. The entire root-finding process, commonly referred to as the "secant method," was programmed for a digital computer. The program (see fig. 6) ran until the difference between the current estimate and old estimate became too small to detect. When the computer printed "division by zero error" (see fig. 7), the last computed $g_{i+1}$ value was taken as the true root.

The polynomial P has an infinite number of roots; however, the computer converges on the root nearest the starting values. As an example, consider the two runs shown on figure 7. The runs were based on the same value for f, namely 3.0, but different starting values for g. For the first run, g was started at 6: for the second run, g was started at 3. Despite this difference, both runs converged on the same g-root--namely 5.34273357. Because the computer stored all numbers to nine decimal places, each g root was accurate to the seventh or possibly the eighth decimal place. Many runs were made to insure all roots of interest were found.

The relation between f and three of the g roots is shown on figure 8. For a given f value, the smallest g root lies on the curve labeled $g_1$ and

```
 1  D$ = " ":REM CONTROL D
 3  HOME
 5  PRINT "THIS PROG PERTAINS TO THE VIBRATIONAL-FREQUENCY EQUATION FOR A
      TUBE SUBJECTED TO AN AXIAL FORCE"
 7  PRINT "ROOTS OF THE EQUATION ARE FOUND BY THE SECANT METHOD.  ONE ROOT,
      F, IS ASSIGNED AND THE OTHER ROOT, G, IS COMPUTED" BY ITERATION.
10  PRINT "ENTER VALUE OF F"
15  INPUT F
25  PRINT D$; "PR#1"
30  PRINT "VALUE OF ROOT F IS ";F

40  PRINT D$; "PR#0"
45  PRINT "ENTER ESTIMATED VALUE OF SECOND ROOT G"
50  INPUT XC
55  PRINT "ENTER A VALUE NEARLY EQUAL TO THE PRECEEDING INPUT"
60  INPUT XO
61  HOME
62  PRINT "ESTIMATE OF";"    ";"VALUE OF"
63  PRINT "ROOT    ";"    ";"EQUATION"
65  G = XC
70  GOSUB 1000
75  PC = P
80  G = XO
85  GOSUB 1000
90  PO = P
100 N = XC - XO
110 D = PC - PO
120 XN = XC - PC * (N / D)
130 REM END OF SECANT COMP
140 G = XN
150 GOSUB 1000
160 PN = P
165 PRINT XN;"    "PN
280 REM START UPDATE
290 XO = XC
300 XC = XN
320 GOTO 65
350 END
1000 R = 1 - G ^ 2 / F ^ 2
1010 T = ( - 2) * G / F
1020 S = EXP (F) - EXP ( - F)
1030 U = EXP (F) + EXP ( - F)
1040 V = 4 * G / F
1050 P = R * S *  SIN (G) + T * U * COS (G) + V
1070 RETURN
```

Figure 6.--Program listing for the secant method.

```
ENTER VALUE FOR F
ENTER ESTIMATED VALUE FOR ROOT G
?6
ENTER A VALUE NEARLY EQUAL TO THE PRECEEDING INPUT
?6.1
NEW ESTIMATE OF    VALUE OF
ROOT G             EQUATION
5.37467885        -2.28601221
5.34623264        -.248477478
5.34276362        -2.13186815E-03
5.3427336        -1.95018947E-06
5.34273357        -9.87201929E-08
5.34273357        1.3038516E-07
5.34273357        -9.87201929E-08
5.34273357        -9.87201929E-08

?DIVISION BY ZERO ERROR IN 120
```

```
]VALUE OF ROOT F IS 3
ENTER ESTIMATED VALUE OF SECOND ROOT G
?3
ENTER A VALUE NEARLY EQUAL TO THE PRECEEDING INPUT
?5
NEW ESTIMATE OF     VALUE OF
ROOT G              EQUATION
6.97285063        -119.033626
4.06984791        51.6438111
4.94824242        24.5948866
5.7469438        -31.325129
5.29952934        3.02813778
5.33896759        .266898096
5.34277965        -3.26870568E-03
5.34273352        3.41795385E-06
5.34273357        -9.87201929E-08
5.34273357        1.3038516E-07
5.34273357        -9.87201929E-08
5.34273357        -9.87201929E-08

?DIVISION BY ZERO ERROR IN 120
```

Figure 7.--Sample outputs from the secant-method program.

the next larger root lies on the curve labeled $g_2$. The third root, taken in order of ascending magnitude, lies on the curve labeled $g_3$.

Each of the g-root curves lies between asymptotic limits. For example, as we assign smaller and smaller values to f, $g_1$ increases and approaches $2\pi$. If we reverse the process by assigning larger and larger values to f, $g_1$ decreases and approaches $\pi$.

## Special Solutions of the Tension Equation

In this section, we compare special solutions of the tension equation with results obtained by other investigators. However, before this comparison can be made, the f-g roots must be linked to physical parameters of vibrating tubes.

Earlier, we saw that the form of equation 8 matches the form of equation 6 if $a'=-a$. By substituting this relation into equation 8 and eliminating $a'$, we obtain

$$D^4 - (a^2 - b^2)D^2 - a^2b^2 = 0 \tag{27}$$

Equating the $D^2$ coefficient in equation 6 to the $D^2$ coefficient in equation 27 yields

$$a^2-b^2 = S/EI \tag{28}$$

Equating the $D^0$ coefficient in equation 6 to the $D^0$ coefficient in equation 27 yields

$$a^2b^2 = rp^2/EI \tag{29}$$

Because $a=f/L$ and $b=g/L$ (see equations 17 and 18), we can rewrite equation 28 as

$$f^2 - g^2 = SL^2/EI \tag{30}$$

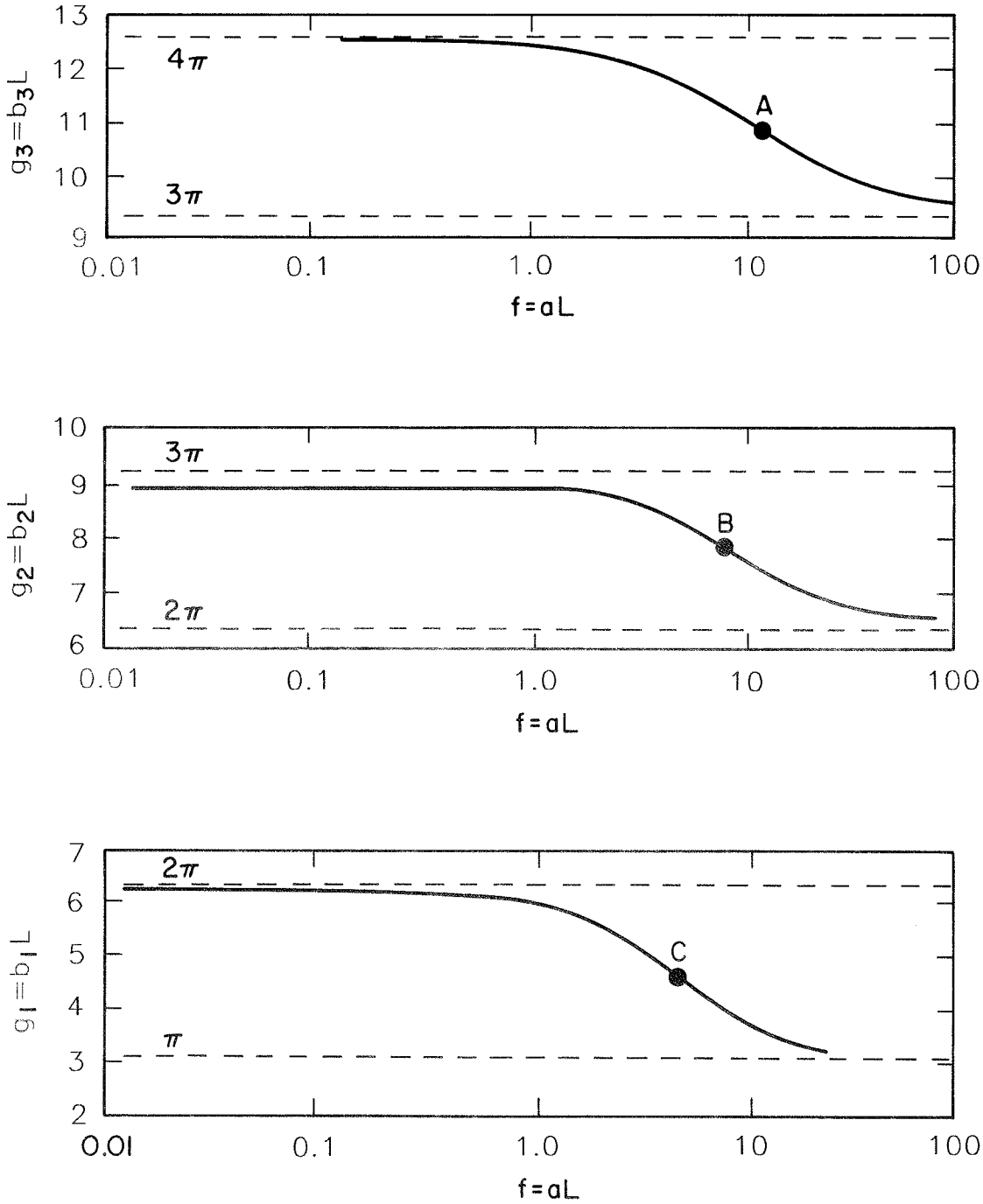


Figure 8.--Roots of the tension equation. A, B, and C locate equal roots. At A, $g_3 = f = 10.9956078$. At B, $g_2 = f = 7.85320463$. At C, $g_1 = f = 4.73004075$.

and equation 29 as

$$f^2g^2 = L^4rp^2/EI \tag{31}$$

Taking the square root of both sides of equation 31 yields

$$fg = pL^2/\sqrt{EI/r} \tag{32}$$

Equations 30 and 32 are graphed on figure 9. Points on the curve labeled "n = 1" were obtained by first selecting an arbitrary value for f, and then reading the matching $g_1$ value from figure 8. Finally, values for the expressions $f^2-g_1{}^2$ and $fg_1$ were computed and plotted against one another. Points on the n = 2 curve were obtained in a similar manner. The only difference was that $g_2$ values instead of $g_1$ values were read from figure 8.

Curves on figure 9 are related to the modal shapes on figure 1. A tube vibrates at its lowest frequency, $p_1$, when the tube's modal shape matches figure 1a. The frequency $p_1$ together with values for E, I, L, and S set an operating point on the n = 1 curve of figure 9. If S = 0, the operating point lies at the intersection of the n = 1 curve and the vertical axis separating tension from compression regions. The same tube vibrates at a higher frequency, $p_2$, when the modal shape matches figure 1b. If S = 0, the operating point lies at the intersection of the n = 2 curve and the vertical axis. The tube vibrates at an even higher frequency, $p_3$, when the modal shape matches figure 1c. If S = 0, the operating point lies at the intersection of the n = 3 curve and the vertical axis.

Let us examine the special case in which the tube is free of axial forces. Equation 30 shows that if S = 0 then f = g. The bottom curve on

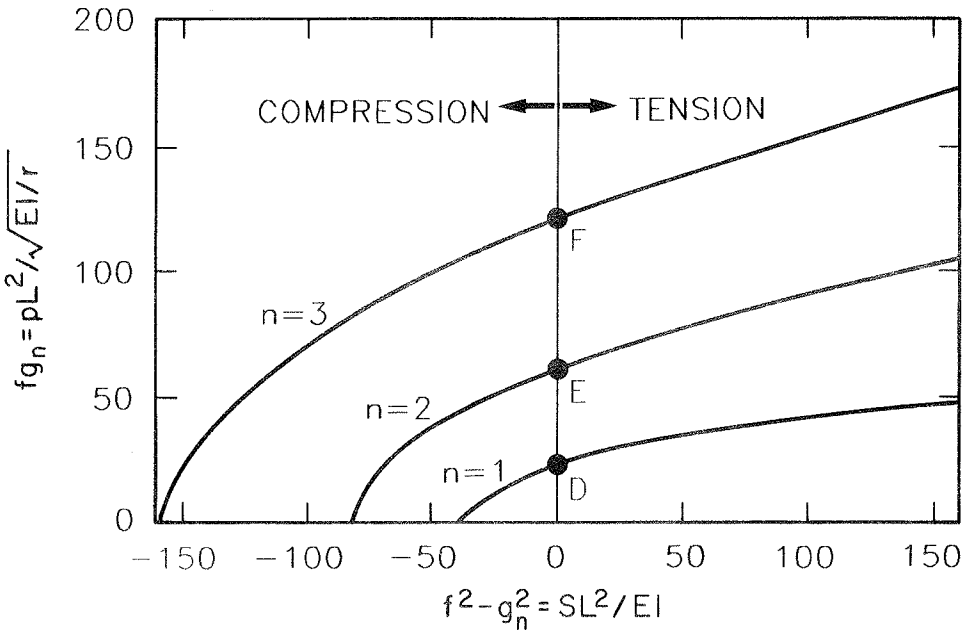


Figure 9.--Tension-compression regions for three modes of vibration.

figure 8 shows that f equals $g_1$ at only one point. Both parameters equal 4.73004075. Squaring this value we obtain 22.373286 for $fg_1$, the ordinate of point D on figure 9. Following a similar line of reasoning, we obtain 61.672823 for $fg_2$ (point E on figure 9) and 120.903391 for $fg_3$ (point F on figure 9). Table 1 lists these three $fg_n$ values and compares them with values cited by Rothbart (1964) and Lalanne (1983). Notice that data from all three sources agree closely.

Table 1.--Comparison of vibrational frequencies for the special case S = 0.

| | Source of Data | | |
|---|---|---|---|
| Frequency | Figure 9 | Rothbart | Lalanne |
| $p_1$ | 22.373286(Z)(1) | 22.37(Z) | 22.37(Z) |
| $p_2$ | 61.672823(Z) | 61.62(Z) | 61.67(Z) |
| $p_3$ | 120.903391(Z) | 120.(Z) | 120.9 (Z) |

(1) $Z = \sqrt{EI/rL^4}$

Let us now examine another special case in which a tube is subjected to compressive forces. To this point in the discussion, S has been treated as a tensive force as shown by the vector on figure 2b. We can make S a compressive force by substituting −S for +S. On figure 9, operating points with negative S values plot left of the vertical axis.

Tubes subjected to compressive forces have a vibrational property that

can be studied experimentally with the aid of a yardstick or a straight, slender rod. With the stick standing upright with its bottom end resting on the floor, apply a small downward force on the top end. The stick remains straight but as the force slowly increases, the load reaches a critical value and the stick buckles (bows sideways). The magnitude of this critical force depends on the way in which the stick's ends are supported. If both ends are clamped so they remain plumb even after the center section buckles, the critical force, which was derived by Laurson and Cox (1947), is

$$S_{cr} = 4\pi^2 EI/L^2 \tag{33}$$

Compressive forces not only cause buckling but they also influence vibrational frequencies. The influence can be gaged by running another experiment on the yardstick. While maintaining small but steady downward force on the top end, pull the center of the stick sideways and then release the stick to excite the first mode of vibration. Repeating this test with greater and greater downward forces reveals two things: (a) as compressive force increases, vibrational frequency decreases and (b) when compressive force equals or exceeds $S_{cr}$, vibration stops or, stated another way, vibrational frequency becomes zero.

The experimental trend of the force-frequency relation agrees with the theoretical trend on figure 9. Increasing the compressive force shifts the operating point left and downward along the $n = 1$ curve. This shift is accompanied by a decrease in frequency. When the operating point reaches the horizontal axis, frequency becomes zero.

On figure 9, the point where the $n = 1$ curve intersects the horizontal axis is related to $S_{cr}$ in equation 33. According to figure 9, $fg_1$ is zero

since the point falls on the horizontal axis; however, according to figure 8, $g_1$ can never be smaller than about 3. To reach the point, f must approach zero and $g_1$ must approach $2\pi$. As we approach these limits, $f^2-g^2$ approaches $-4\pi^2$, the point's abscissa on figure 9. Glancing at the horizontal-axis variable, we see the following condition is met:

$$SL^2/EI = -4\pi^2 \tag{34}$$

Solving equation 34 for S yields $-4\pi^2EI/L^2$. Except for a difference in sign, this expression is identical to the right-hand expression in equation 33. The difference in sign stems from a difference in definitions; Laurson and Cox define a compressive force as positive but we define a compressive force as negative.

Let us now focus on one more special case that applies to long, slender, tightly-stretched strings. DenHartog (1947) derived the equation

$$p_n = (n\pi/L)(\sqrt{S/r}) \tag{35}$$

where $p_n$ is the frequency of a string vibrating in its $n^{th}$ mode. The variable n takes on the values 1, 2, 3, etc. DenHartog's equation can be derived from equations 30 and 31 and data from figure 8. First, we solve equation 30 for EI to obtain

$$EI = (SL^2)/(f^2-g^2) \tag{36}$$

Substituting the expression for EI into equation 31 and then solving for p gives

$$p = [fg/\sqrt{f^2-g^2}][\sqrt{S/rL^2}] \tag{37}$$

Now consider a string having a fixed value for $L^2/EI$ and acted upon by a slowly increasing tensive force. As S increases, $SL^2/EI$ increases and the string's operating point shifts to the right along the curves of figure 9.

As this shift continues, $f^2-g^2$ increases and, according to figure 8, f becomes much larger than g. In the limit the expression inside the left-hand braces of equation 37 approaches g. Figure 8 shows that $g_1$ approaches $\pi$, $g_2$ approaches $2\pi$, and $g_3$ approaches $3\pi$: in general, $g_n$ approaches $n\pi$. DenHartog's equation is obtained by substituting $n\pi$ for the expression in the left braces of equation 37.

In summary, results from the tension equation agree with three special-case studies reported by other investigators. These studies cover (a) tubes free of all axial forces, (b) tubes subjected to critical buckling forces and, (c) tubes (or strings) subjected to large tensive forces. In the next section, we compare theoretical data from the tension equation with experimental data from an experimental sediment-concentration gage.

## ANALYSIS OF EXPERIMENTAL DATA

Figure 10 shows details of a straight-tube sediment-concentration gage. The guide vanes align the nose with the approaching flow so that water enters the tube and then emerges downstream of the vanes. The hatch, which can be removed for servicing parts inside the sleeve, forms an airtight cover. The gas valve can be connected to a vacuum pump for removing air inside the sleeve.

The tube is welded at three points--two at the front cap and one at the rear cap. Each of these welds forms a continuous band around the tube's circumference. Although the tube cannot move at the welds, it can vibrate in the span labeled "L" on section BB. Two coils--one labeled "drive" and the other labeled "sense"--are located at the center of the span. The coils

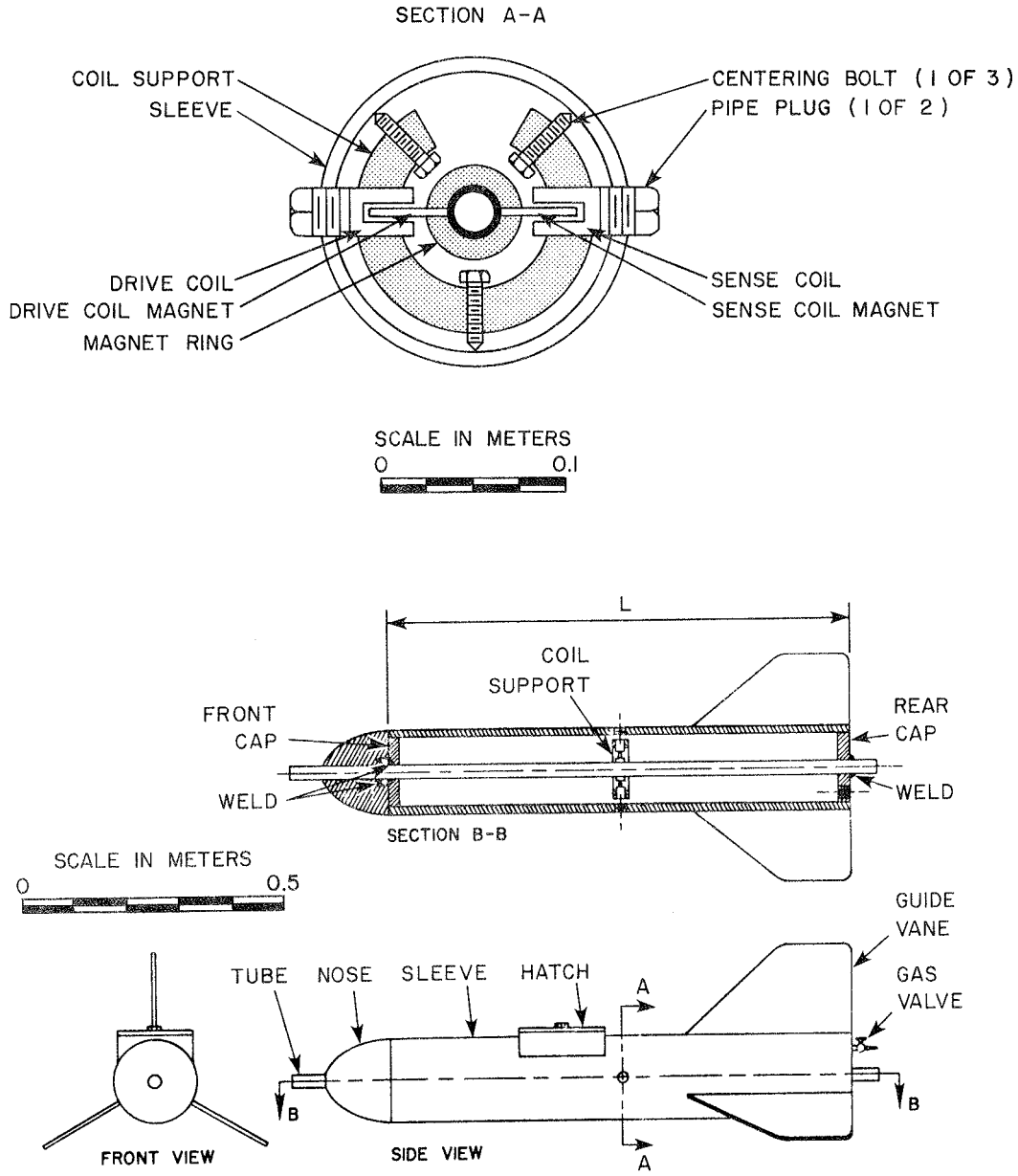


Figure 10.--Straight-tube sediment gage.

surround but do not touch the slender, rod-shaped magnets shown in section AA. The magnets are fastened to the magnet ring which, in turn, is brazed to the tube. The tube vibrates along the horizontal center line shown in section AA. The magnet ring and magnets vibrate as a unit but the coils remain stationary.

An electronic amplifier, which is not shown, sustains the vibration. The amplifier's input terminals are connected to the sense coil and the amplifier's output terminals are connected to the drive coil. Vibration of the sense-coil magnet produces an electrical signal that is amplified and then applied to the drive coil. The drive-coil voltage produces a magnetic field that exerts a force on the drive-coil magnet. The feedback process is regenerative--motion produces signal, signal produces force, and force produces motion.

The permanent magnet in the drive coil plays a critical role in transforming electric current to force. Two magnetic fields exist in the air-gap between coil and magnet. The magnet's field is strong and steady but the coil's field is weak and its intensity and direction depend on the electric current flowing in the winding. The two fields may oppose one another or they may reinforce one another depending on the direction of current flow. During each vibrational cycle, the current flows first in one direction and then in the opposite direction. The net air-gap flux grows and weakens in step with the current; however, the flux lines never change direction. They always cross the air-gap in a direction set by the permanent magnet. The magnitude of the force on the magnet waxes and wanes in step with the intensity of the net flux but the frequency of the force

always matches the frequency of the current. If the permanent magnet is replaced with a soft-iron core that has no field of its own, the frequency of the force becomes twice the frequency of the coil current. Frequency-doubling, which is undesirable, occurs because the net air-gap flux is governed entirely by the current. When the current reverses, the net flux reverses; consequently, the pulling force on the core reaches two maximums during each vibrational cycle.

The tube (figure 10) vibrates only in its first mode. All other modes are eliminated through mechanical and electrical filtering. Even-numbered modes (see fig. 1b) must have stationary center points, but the tube on figure 10 cannot meet this requirement because driving forces vibrate the center. All odd-numbered modes higher than the first are eliminated because the frequencies are beyond the amplifier's range or because the phasing produces degenerative feedback.

## PARAMETERS FOR THE STRAIGHT-TUBE SEDIMENT GAGE

This section discusses assumptions and approximations used in applying the tension equation to the straight-tube gage on figure 10.

The tension equation was derived for a tube having a uniformly-distributed-mass so we need a way of distributing the concentrated mass of the magnet ring and magnets shown on figure 10. Figure 11 shows a concentrated mass, R, fastened to the center of a uniform tube. Ungar (1964) cites the following equation for the first mode of vibration:

$$p_1^2 = 192.\,EI/(R + 0.375\ Lr)L^3 \tag{38}$$

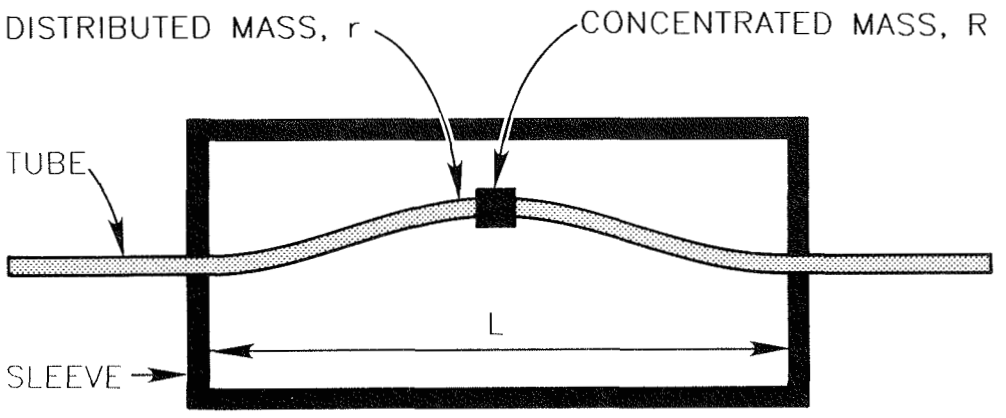


Figure 11.--Tube vibrating in its first mode and carrying a concentrated mass.

This equation can be rewritten as:

$$p_1^2 = 512.EI/[(2.666\ R/L) + r]\ L^4 \tag{39}$$

The bracketed expression in equation 39 is the system's distributed-mass equivalent obtained by adding r for the uniform tube to 2.666 R/L for the concentrated mass. Notice that if R = 0, equation 39 reduces to the $p_1$ expression in table 1.

Later, we will apply the correction 2.666R/L to the magnets and magnet ring, then add the correction to the distributed mass of the steel tube, and the distributed mass of the water and sediment inside the tube.

Let us now consider axial forces produced by temperature shifts. If the welds on figure 10 are cut to free the tube and sleeve from mutually interactive forces, a temperature rise of $\Delta T$ degrees lengthens L by an amount $\Delta L$. The temperature shift and length shift are related by the equation

$$\Delta L = K_t L \Delta T \tag{40}$$

where $K_t$ is thermal coefficient of expansion.

The sleeve is a high-strength carbon-steel alloy with a $K_t$ value of about $12.5 \times 10^{-6}$. The tube is type 304 stainless steel with a $K_t$ value of about $17. \times 10^{-6}$.

Because the sleeve and tube have different $K_t$ values, the temperature shift creates an axial force. To establish the direction of this force, assume the welds are cut while the tube and sleeve are under no axial force. The welds remain aligned with one another. But if the tube and sleeve are now warmed, the tube lengthens more than the sleeve (see equation 40) and the welds shift apart. To realign the welds, the tube must

be compressed and the sleeve must be stretched. After the welds have been rejoined, the tube exerts a tensive force on the shell and the shell exerts a compressive force on the tube.

An axial force produces a deflection (strain) in the sleeve and tube; however, the strain in the sleeve is always small compared to the strain in the tube. The force on the tube is distributed over a small cross-sectional area--about 0.00004 square meters--but the force on the shell is distributed over a much larger area--about 0.0054 square meters.

As we have seen, temperature influences "S" in the tension equation. However, temperature also influences the tube's area moment-of-inertia, given by

$$I = (\pi/4)(r_o^4 - r_i^4) \tag{41}$$

In this equation, $r_o$ and $r_i$ are respectively the tube's outside radius and inside radius. Both of these radii increase if the tube is warmed and they decrease if the tube is cooled.

The following two equations relate a temperature shift dT, to an outer-radius shift $dr_o$ and inner-radius shift $dr_i$:

$$dr_o = K_t r_o (dT) \tag{42}$$

$$dr_i = K_t r_i (dT) \tag{43}$$

Designating I as the area moment of inertia (AMOI) at temperature T and designating dI as the change in AMOI caused by a temperature shift dT, we write

$$dI = [(\partial I/\partial r_o)(\partial r_o/\partial T) + (\partial I/\partial r_i)(\partial r_i/\partial T)]dT \tag{44}$$

Taking partial derivatives of equations 41, 42, and 43, and then

substituting the derivatives into equation 44, we obtain

$$dI = \pi K_t (r_o^4 - r_i^4) dT \tag{45}$$

Substituting the expression for I(equation 41) into equation 45, we

$$4K_t \; I \; dT \tag{46}$$

Designating $I_{T+\Delta T}$ as the AMOI at $T+\Delta T$, we obtain

$$I_{T+\Delta T} = I_T + dI \tag{47}$$

After substituting equation 46 into equation 47 and then simplifying the result, we obtain

$$I_{T+\Delta T} = I_T(1+4K_T\Delta T) \tag{48}$$

Equation 48 is useful because it enables us to compute the AMOI at $T + \Delta T$ from the AMOI at T.

We can now evaluate vibrational constants for the gage on figure 10. Values for "water density" (see table 2) were taken from Hodgman (1910). Values for L were obtained by first measuring the distance between welds (see fig. 10) at $20^{\circ}$ C and then using equation 40 to evaluate lengths for all other temperatures in the table. In equation 40, $K_t$ was taken as $12.5 \times 10^{-6}$. Values for "inside diameter of tube" were obtained by first measuring the diameter at $0^{\circ}$ C and then using equation 40 to evaluate diameters for other temperatures in the table. Values for "cross-sectional area of tube bore" were computed from the equation $A = \pi d_i^2/4$.

Table 2.--Vibrational constants for various temperatures. All values are for the gage on figure 10. E(tube's elastic-modulus) = 193. x $10^9$ $N/m^2$ for all temperatures.

| T, temperature in degrees Celsius | Water density, in $Kg/m^3$ | L, tube length in meters | $r_i$, inside diameter of tube, in meters |
|---|---|---|---|
| 0 | 999.87 | 0.90805 | 0.024384048 |
| 10 | 999.73 | 0.90816 | 0.024388193 |
| 20 | 998.23 | 0.90827 | 0.024392338 |
| 30 | 995.67 | 0.90838 | 0.024396483 |
| 40 | 992.24 | 0.90849 | 0.024400628 |

| T, temperature in degrees Celsius | Cross-sectional area of tube bore in $m^2$ | I, moment of inertia of tube in $m^4$ | $r_{tube}$, distributed mass of tube, in Kg/m |
|---|---|---|---|
| 0 | 0.000466983 | $3.0781320 \times 10^{-9}$ | 0.31860309 |
| 10 | 0.000467142 | $3.0802251 \times 10^{-9}$ | 0.31856449 |
| 20 | 0.000467301 | $3.0823182 \times 10^{-9}$ | 0.31852590 |
| 30 | 0.000467460 | $3.0844114 \times 10^{-9}$ | 0.31848735 |
| 40 | 0.000467619 | $3.0865045 \times 10^{-9}$ | 0.31844878 |

| T, temperature in degrees Celsius | $r_{concentrated}$, distributed mass of ring and magnets in Kg/m | $r_{water}$, distributed mass of water, in Kg/m | r, total distributed mass, in Kg/m |
|---|---|---|---|
| 0 | 0.4454663 | 0.466922290 | 1.23099168 |
| 10 | 0.4454123 | 0.467015872 | 1.23099268 |
| 20 | 0.4453534 | 0.466473877 | 1.23035324 |
| 30 | 0.4453044 | 0.465435898 | 1.22922769 |
| 40 | 0.4452505 | 0.463990277 | 1.22768959 |

Values for I, "moment-of-inertia of tube" were computed from equations 41 and 48 along with measurements of $r_i$ and $r_o$ at $0^o$ C. Values for $r_{tube}$ were obtained by dividing the mass of the tube between welds (0.31860309 Kg) by L. Values for $r_{concentrated\ mass}$ were obtained from the expression 2.666(0.15169)/L (see equation 39). The value in parenthesis is the mass in Kg of the magnet-ring assembly.

Each value for $r_{water}$ was computed from the volume of a one-meter length of the tube. The volume was then multiplied by the concomitant water-density value in the table. Values for "r" were computed from the equation, $r = r_{concentrated} + r_{tube} + r_{water}$.

Most of the values in table 2 contain more decimal places than measurements warrant. For example, L is given to five decimal places but these values are based on a measurement that was accurate to only four decimal places. Extra decimal places are cited to show small shifts in the vibrational constants.

## COMPARISON OF MEASURED FREQUENCIES AND THEORETICAL FREQUENCIES

Szalona (1986) measured vibrational frequencies for the gage on figure 10. The gage was submerged in a water bath connected to a temperature-controlled reservoir of sediment-free water. After the water bath, reservoir, sleeve, and tube had all stabilized at the same temperature, the tube's vibrational frequency was recorded. The water was then warmed a few degrees. After a restabilization period, another frequency reading was collected. As figure 12 shows, the measured-frequency data plotted along a nearly-straight line having a negative slope.

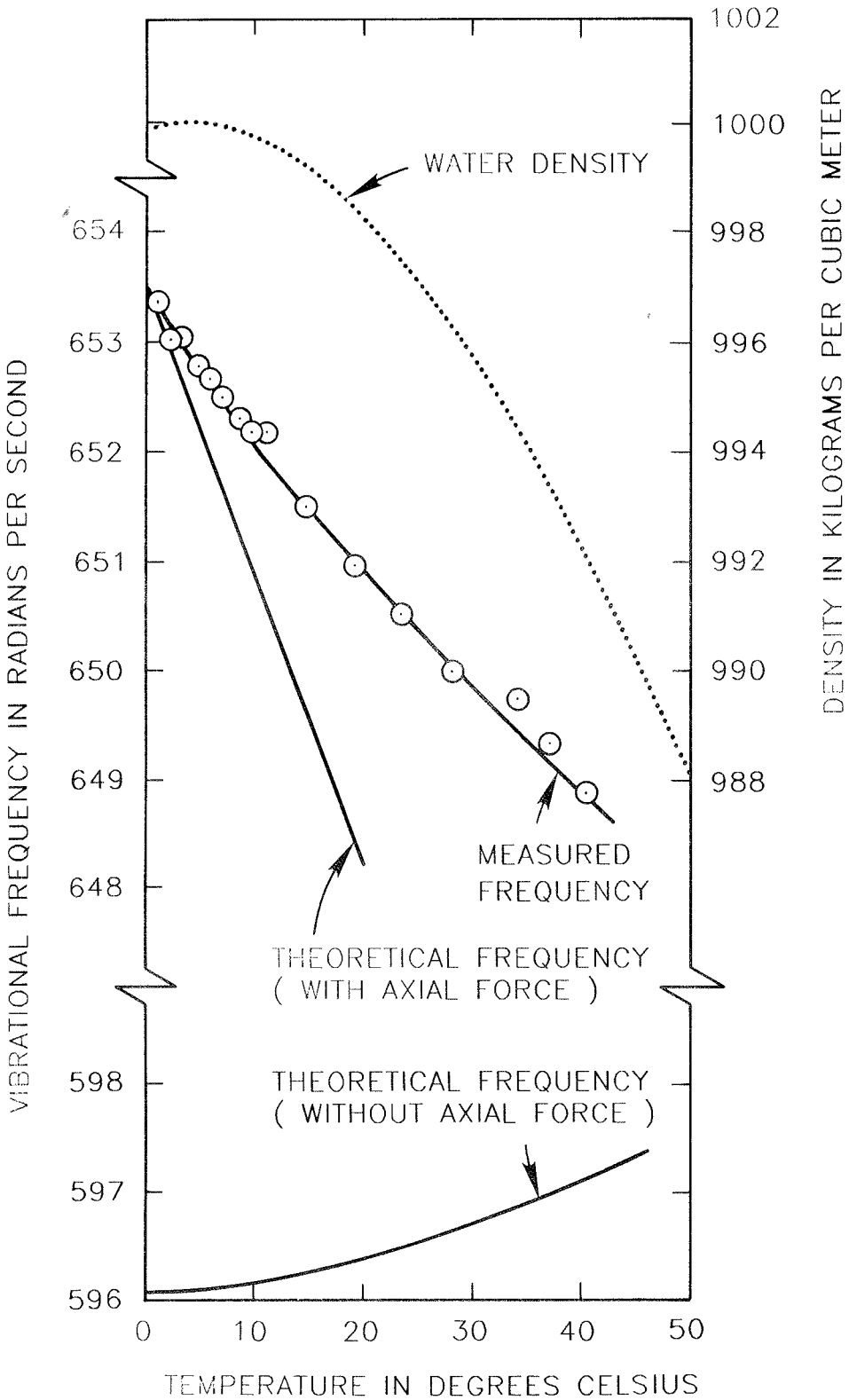


Figure 12.--Comparison of measured and theoretical frequencies.

The trend of the measured data shows temperature exerts a strong influence on metallic parts of the gage. Assume, for the moment, that the gage responds only to shifts in water density. Figure 12 shows that water reaches its maximum density at $4^{\circ}$ C. Starting at this temperature, a warming trend has the same effect as a cooling trend--density decreases and vibrational frequency increases. Frequency data would therefore plot along a bowl-shaped curve (concave upward) instead of a straight, downward-sloping line.

Temperature induced shifts in L, I, and r can be studied by using the tension equation and values from table 2. First, consider the special case, S = 0. At all temperatures, the tube operates at the point on figure 13 where the n = 1 curve crosses the vertical axis. At this point

$$pL^2/\sqrt{EI/r} = 22.373286 \tag{49}$$

Substituting values for E, I, r, and L (see table 2) into equation 49 and then solving the equation for p yields points on the bottom curve of figure 12. Comparing this theoretical curve with the measured-data curve on figure 12 reveals two discrepancies: (a) the theoretical curve plots below the measured curve and (b) the theoretical curve has a positive slope but the measured curve has a negative slope.

What happens to frequency discrepancies if S takes on non-zero values? Because S was not measured, we must estimate its value by reverse calculating. First, values for E, I, r, and L at $0^{\circ}$ C (table 2) and the measured frequency at $0^{\circ}$ C (653.5 radians per second) are substituted into equation 32. We obtain $fg_1 = 24.53$. Then, opposite $fg_1$ on figure 12, we read $SL^2/EI = 8.0$. Solving this equation for S and then substituting

values for E, I, and L, yields S = +5763 newtons (+1296 pounds). The positive sign indicates the tube is under tension at $0^{o}$ C.

If the tube and shell are warmed, S decreases. The change in S can be computed by assuming the tube and shell are free to expand independently. If both parts are warmed to $40^{o}$ C, the tube's length changes by $(17. \times 10^{-6})$ (0.90805)(40) = 617 micrometers and the sleeve's length changes by $(12.5 \times 10^{-6})$ (.90805)(40) = 454 micrometers. The tube must now be compressed 163 micrometers to rejoin the welds. The required compressive force $\Delta S$ is obtained from the equation:

$$E = \text{stress/strain} = (\Delta S/A)/(\Delta L/L) \tag{50}$$

In this equation, A is the tube's cross-sectional area, L is the tube's length, $\Delta S$ is the applied force, and $\Delta L$ is the change in tube length. Solving equation 50 for $\Delta S$ and then substituting $193. \times 10^{9}$ for E, $163 \times 10^{-6}$ for $\Delta L$, $39.73 \times 10^{-6}$ for A, and 0.90805 for L, yields $\Delta S$ = 1376 newtons. Because the relation between $\Delta S$ and $\Delta T$ is linear, we write

$$\Delta S = (\Delta T)(-1376/40) \tag{51}$$

where $\Delta T$ is in degrees Celsius and $\Delta S$ is in newtons.

Frequencies for a range of temperatures can now be computed. For example, assume temperature shifts from $0^{o}$ C to $10^{o}$ C. According to equation 51, S decreases by 340 newtons. With S at 5423 newtons, $f^2 - g_1{}^2$ (see figure 13) becomes 7.52 and $fg_1$ becomes 24.41. Solving equation 32 for $p_1$ yields 650.9 radians per second. The relation between $p_1$ and T is closely approximated by the straight line labeled "theoretical frequencies with axial forces applied" on figure 12.

Figure 12 shows this new theoretical plot and the measured-frequency plot have two features in common: both plots are nearly straight and both have negative slopes. Tension apparently plays a significant role in controlling the gage's frequency.

## TEMPORAL SHIFTS IN FREQUENCY

Earlier, we computed a tensive force of 5763 newtons in the tube. The origin of this large force is a matter of speculation since no deliberate effort was made to stretch the tube during assembly. The force was probably created by high temperatures used in welding. Points inside the welds were heated to about 1400° C --the melting temperature of stainless steel--but points outside the welds remained cooler. For computational purposes, let us take 150° C as the average temperature along the sleeve and 800° C as the average temperature along the tube. The parts are assigned different temperatures because of contrasting weights and surface areas. Compared to the tube, (a) the sleeve has a larger mass and consequently warms at a slower rate and (b) the sleeve has a larger surface area and consequently radiates heat at a faster rate.

After all welds were complete, the tube and sleeve were allowed to cool. We can estimate forces that developed during the cooling process by working with initial and final conditions. For initial conditions, assume (a) the sleeve and tube temperatures were 150° C and 800° C respectively, (b) the sleeve and tube were locked together but neither part was under stress and (c) the distance between welds was 0.91032 meters. For final conditions, assume the sleeve and tube were at a temperature of 0° C.

According to equation 40, the sleeve's final length was 0.90805 meters and the tube's final length was 0.89794 meters. The difference between these two lengths is critical. Stretching the tube 0.01011 meters requires a force of about 86,000 newtons (19,000 pounds). Dividing this force by the cross-section area of the tube gives about 2. x $10^9$ newtons/$m^2$--a stress that exceeds elastic limits for stainless steel!

The existence of hyperelastic stresses is affirmed by some experimental data. A few days after cooling, the gage's vibrational frequency was 724 radians/second; five months later, the frequency was 651. radians/second. Metals subjected to hyperelastic stresses tend to lengthen at slow rates. Gela (1964) states the lengthening process may continue for months or even years. In the experimental gage, stretching would have reduced tensive forces and shifted the tube's operating point (see figure 13) leftward and downward along the n = 1 curve. These shifts may have caused the frequency reduction.

## CONCLUSIONS

The tension equation is a useful tool for analyzing frequencies in a vibrational-type sediment gage. Roots of the equation are linked to slurry densities and, more importantly, to mechanical properties of the tube itself. These properties include thermal-expansion coefficient, elasticity coefficient, tube diameter, tube length, and tensive force. The equation can be used to select optimum dimensions and properties of critical components in the instrument. Values computed from the equation indicates frequency instabilities observed in the experimental gage were caused by high temperatures used in the welding process.

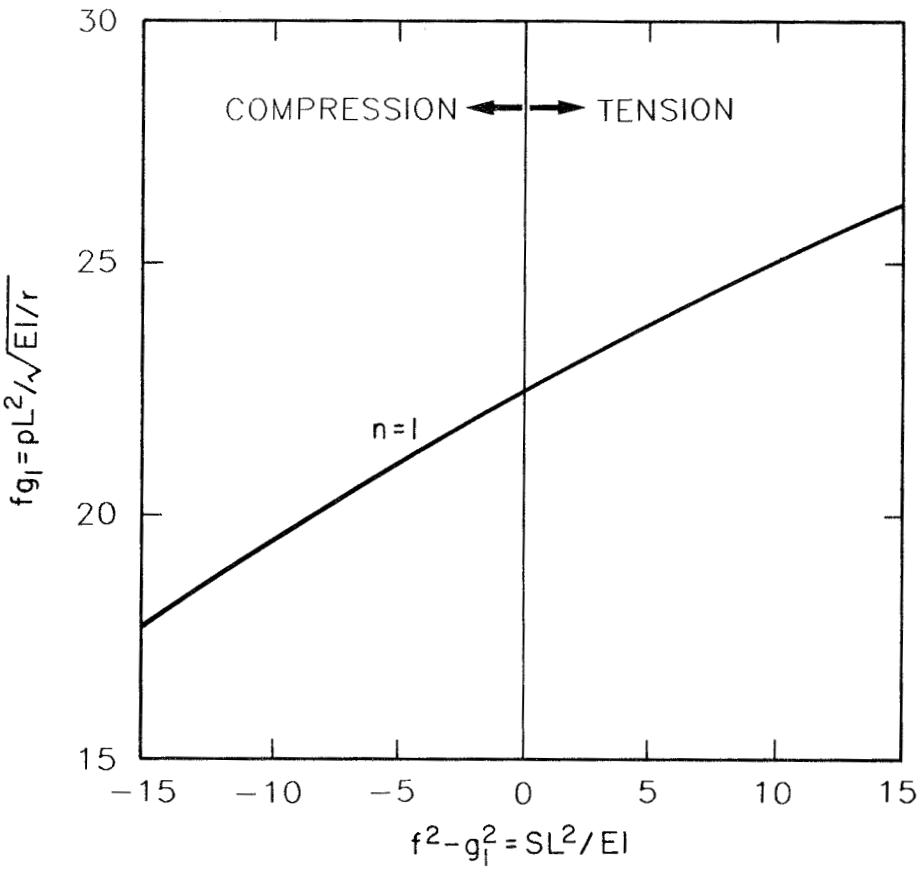


Figure 13.--Detail of tension-compression curve for first mode.

## APPENDIX A - NOTATION

The following symbols are used in this paper:

| | | |
|---|---|---|
| S | Force exerted along the axis of a vibrating tube | N (newtons) |
| x, y | Horizontal and vertical distances in a Cartesian system | m (meters) |
| V | Shear stress in a vibrating tube | $N/M^2$ |
| $r_o$, $r_i$ | Outside radius and inside radius | m |
| r | Total mass per unit length of a vibrating tube | Kg/m (kilogram/m) |
| $r_t$, $r_w$, $r_r$ | Mass per unit length of the tube walls, mass per unit length of the water in the tube, and equivalent mass per unit length of R | Kg/m |
| E | Elastic modulus of the tube | $N/m^2$ |
| e | Base of natural logrithims | |
| I | Area moment-of-inertia | $m^4$ |
| X | A function of x that defines the elastic curve for a vibrating tube | m |
| t | Time | s (seconds) |
| j | The imaginary operator, $\sqrt{-1}$ | |
| p | Angular frequency | radians/s |
| $C_1$, $C_2$, $C_3$, $C_4$ | Coefficients of terms in the modal shape equation X. | |
| L | Free length of a vibrating tube | m |
| R | Mass concentrated at the mid-point of a vibrating tube | Kg |

| | | |
|---|---|---|
| D | Differential operator d/dt | |
| a, jb, -a, -jb | Roots of the auxiliary equation | |
| f, g | Coefficients in the tension equation, $f = aL$ and $g = bL$ | |
| T | Coefficient of thermal expansion | micrometers/m/ per $^{o}$ C |
| A | Cross section area based on the inside diameter of the vibrating tube | $m^2$ |
| M | Bending moment in the vibrating tube | Kg-m |

## REFERENCES


DenHartog, J. P., 1947, Mechanical vibrations (3rd): New York, McGraw-Hill, p. 175.

Gela, T. D., 1964, Properties of engineering materials, in Rothbart, H. A., ed., Mechanical design and systems handbook: New York, Mcgraw-Hill, sec. 17-26.

Hodgman, C. D., 1910, Handbook of chemistry and physics, (30th ed.): Chemical Rubber Publishing Company, p. 1694.

Lalanne, M., Berthier, P., and Der Hagopian, J., 1983, Mechanical vibrations for engineers: New York, John Wiley Interscience, p. 103.

Laurson, P. G., and Cox, W. J., 1947, Mechanics of materials (2nd ed.): New York, John Wiley, p. 157, 227.

Leighton, W., 1952, An introduction to the theory of differential equations: New York, Mcgraw-Hill, p. 47.

Rothbart, H. A., ed., 1964, Mechanical design and systems handbook: New York, Mcgraw-Hill, sec. 6-38.

Rothenberg, R. I., 1983, Linear algebra with computer applications: New York, John Wiley, p. 100, 116.

Skinner, J. V., Beverage, J. P., and Goddard, G. L., 1986, Continuous measurement of suspended-sediment concentration: Fourth Federal Interagency Sedimentation Conference, Las Vegas, Nev., 1986, Proceedings.

Szalona, J. J., 1986, Progress report: Description and test of a straight-tube fluid-density gage for measuring suspended-sediment concentration in streams, Report HH of A study of methods used in measurement and analysis of sediment loads in streams: Minneapolis, Minn., Interagency Advisory Comm. on Water Data, Federal Interagency Sedimentation Project.

Timoshenko, S., Young, D. H., and Weaver, W., Jr., 1974, Vibration problems in engineering (4th ed.): New York, John Wiley, p. 454.

Ungar, E. E., 1964, Mechanical vibrations, in Rothbart, H. A., ed., Mechanical design and systems handbook: New York, McGraw-Hill, sec. 6-54, 6-67.